AIAA 2005-4001

Verification and Validation of Rocket Stability Integral Transformations

S. R. Fischbach, J. Majdalani and G. A. Flandro
Advanced Theoretical Research Center
University of Tennessee Space Institute
Tullahoma, TN 37388

J. C. French
Software and Engineering Associates, Inc.
Carson City, NV 89701

41st AIAA/ASME/SAE/ASEE Joint Propulsion Conference and Exhibit
10–13 July 2005
Tucson, AZ

41st AIAA/ASME/SAE/ASEE Joint Propulsion Conference and Exhibit
10-13 July 2005, Tucson, Arizona

AIAA 2005-4001

Verification and Validation of Rocket Stability Integral Transformations

Sean R. Fischbach,[*] Joseph Majdalani,[†] and Gary A. Flandro[‡]
University of Tennessee Space Institute, Tullahoma, TN, 37388

and

Jonathan C. French[§]
Software and Engineering Associates Inc., Carson City, NV, 89701

This paper presents affirmation of the work we have performed to improve upon current combustion instability predictive capabilities. Recently, the ten stability integrals presented by Flandro and Majdalani (Flandro, G. A., and Majdalani, J., "Aeroacoustic Instability in Rockets," *AIAA Journal*, Vol. 41, No. 3, 2003, pp. 485-497) have been converted from volume to surface form for the purpose of implementation into the Standard Stability Prediction (SSP) algorithm. The necessity for converting from volume to surface form is due to the difficulties in calculating the vortical unsteady flowfield throughout the chamber volume. The properties of the flowfield are more accurately defined on the motor surface boundaries and will therefore lead to a more precise assessment of the motor's propensity for instabilities. The surface integrals also allow for substitution of the vortical unsteady velocity with the acoustic counterpart via the no-slip condition. The latter is much easier to compute. Conversion therefore allows for the evaluation of stability factors with the use of only the acoustic pressure and its gradients. In this study we use both asymptotic and numerical techniques in evaluating the ten rocket stability integrals in surface and volume forms. Numerical calculations are performed for the three representative cases and two baseline geometries: (1.) the circular-port and (2.) rectangular slab motors. All results are compared and tabulated. Calculations made in house are also compared to the estimates gained from SSP and shown to be concurrent.

Nomenclature

A_p	=	unsteady pressure amplitude
$A_b^{(r)}$	=	burning surface admittance
$A_S^{(r)}$	=	inert surface admittance
$A_N^{(r)}$	=	nozzle entrance plane admittance
a_0	=	mean speed of sound
E	=	time averaged unsteady system energy
E_m^2	=	energy normalization function for mode m
$\boldsymbol{e}_r, \boldsymbol{e}_\theta, \boldsymbol{e}_z$	=	unit vectors in r, θ and z directions
F	=	body forces
k_m	=	wave number for axial mode m

[*]Graduate Research Associate, Department of Mechanical, Aerospace and Biomedical Engineering. Student Member AIAA.
[†]Jack D. Whitfield Professor of High Speed Flows, Department of Mechanical, Aerospace and Biomedical Engineering. Member AIAA.
[‡]Boling Chair Professor of Excellence in Propulsion, Department of Mechanical, Aerospace and Biomedical Engineering. Member AIAA.
[§]Senior Research Scientist. Member AIAA.

L , R = enclosure length and radius, $l = L/R$
m = oscillation mode shape number
$\boldsymbol{n}$ = outward pointing unit normal vector
p_0 = mean pressure
r , z , t = radial, axial, and temporal coordinates
S = Strouhal Number, k_m / M_b
$\boldsymbol{u}$ = total velocity vector
U_r , U_z = mean flow velocities normalized by V_b
x = action coordinate, $\frac{1}{2}\pi r^2$
y = radial distance from the wall, $1-r$
α = growth rate (dimensional, $\sec^{-1}$)
δ = viscous number, $[\nu/(a_0 R)]^{1/2}$
ε = wave amplitude, $A_p/(\gamma p_0)$
ϕ = function defined in references[1,2]
γ = ratio of specific heats
ν = kinematic viscosity, μ/ρ
ρ = density
ω , Ω = unsteady and mean vorticity magnitudes
ψ = exponential argument defined in references[1,2]

Subscripts

b = refers to the burning/transpiring surface
i , r = irrotational or rotational
m = for a given mode number
N , S = nozzle or inert surface
' = a fluctuating term

Superscripts

* = dimensional quantity
$\sim$, ^ = rotational or acoustical part
r , i = part of a complex variable

I. Introduction

THIS study seeks to impart additional validity to recent developments in the combustion instability algorithm utilized in the Standard Stability Prediction Program (SSP) and employed by the propulsion industry for prognostic insight. Recent studies by Flandro and Majdalani[3,4] have resulted in a more comprehensive combustion stability formulation utilizing both irrotational (acoustic) and rotational (vortical) flow variables. This was accomplished by implementing unsteady rotational flow terms at the ground level and retaining such terms throughout the linear stability analysis. The improved methodology invokes spatial and temporal averaging methods that bring about ten volume integrals denoted as stability growth rates. The summation of these ten stability integrals represents the exponential growth (or decay) of oscillatory energy within the combustion chamber. A study performed by Fischbach, Flandro and Majdalani[5] has successfully converted the ten volume integrals into more amenable surface forms. The outcome of that study is presented in Table 1. The necessity for conversion emanates from the complexities of the solenoidal (rotational) flowfield. Integration of unsteady rotational flow terms over the chamber volume is an extremely daunting problem that is costly in both computer resources and accuracy. Confining the integration to the chamber surfaces greatly simplifies the evaluation of the individual stability factors, while making full use of the acoustic flowfield. Surface integrals enable us to evaluate the individual growth rate factors while only knowing the local pressure and pressure gradients. This removes any ambiguity and consternation that is brought about by attempting to accurately define terms such as the unsteady vorticity throughout the chamber volume. Higher accuracy is entailed through the use of the well-established acoustic terms. As for the integral conversions themselves, they are achieved via the extensive use of vector identities, the divergence theorem, and asymptotic techniques.

Table 1. Rotational integrals in both volumetric and surface integral forms.

	Volumetric form	Surface form	SSP form
E_m^2	$E_m^2 = \frac{1}{2}\iiint[(\hat{p}_m)^2 + \hat{\boldsymbol{u}}_m \cdot \hat{\boldsymbol{u}}_m + 2\hat{\boldsymbol{u}}_m \cdot \tilde{\boldsymbol{u}}_m^i + \tilde{\boldsymbol{u}}_m^r \cdot \tilde{\boldsymbol{u}}_m^r + \tilde{\boldsymbol{u}}_m^i \cdot \tilde{\boldsymbol{u}}_m^i]\mathrm{d}V$		
α_1	$\frac{E_m^{-2}}{\exp(2\alpha_m t)}\iiint_V \left\langle -\nabla\cdot\left[\hat{p}\hat{\boldsymbol{u}} + \frac{1}{2}M_b\boldsymbol{U}(\hat{p})^2\right] - M_b\left[\hat{\boldsymbol{u}}\cdot\nabla(\boldsymbol{U}\cdot\hat{\boldsymbol{u}})\right]\right\rangle \mathrm{d}V$	$\frac{-E_m^{-2}}{\exp(2\alpha_m t)}\iint_S \left\langle \boldsymbol{n}\cdot\left[\hat{p}\hat{\boldsymbol{u}} + \frac{1}{2}M_b\boldsymbol{U}(\hat{p})^2\right] - M_b\left[\boldsymbol{n}\cdot\hat{\boldsymbol{u}}(\boldsymbol{U}\cdot\hat{\boldsymbol{u}})\right]\right\rangle \mathrm{d}S$	$\frac{1}{2}M_b E_m^{-2}\left\{\iint_{S_b}\hat{p}_m^2\left[A_b^{(r)}+1\right]\mathrm{d}S - \iint_{S_N}\hat{p}_m^2\left[A_N^{(r)}+U_N\right]\mathrm{d}S\right\}$
α_2	$\frac{E_m^{-2}}{\exp(2\alpha_m t)}\iiint_V \left\langle \frac{4}{3}\delta^2\hat{\boldsymbol{u}}\cdot\nabla(\nabla\cdot\hat{\boldsymbol{u}})\right\rangle \mathrm{d}V$	$\frac{4k_m\delta^2 E_m^{-2}}{3\exp(2\alpha_m t)}\iint_S\left\langle \boldsymbol{n}\cdot(\hat{p}\hat{\boldsymbol{u}})\right\rangle \mathrm{d}S - \frac{1}{3}\delta^2 E_m^{-2}k_m^2\pi l$	$-\frac{2}{3}k_m\delta^2 E_m^{-2}\left[\iint_{S_b}M_b A_b^{(r)}\hat{p}_m^2\,\mathrm{d}S - \iint_{S_N}M_b A_N^{(r)}\hat{p}_m^2\,\mathrm{d}S + \frac{1}{2}k_m\pi l\right]$
α_3	$\frac{E_m^{-2}}{\exp(2\alpha_m t)}\iiint_V \left\langle M_b\{\hat{\boldsymbol{u}}\cdot(\hat{\boldsymbol{u}}\times\boldsymbol{\Omega})\}\right\rangle \mathrm{d}V$	0	0
α_4	$\frac{E_m^{-2}}{\exp(2\alpha_m t)}\iiint_V \left\langle M_b\hat{\boldsymbol{u}}\cdot(\boldsymbol{U}\times\boldsymbol{\omega})\right\rangle \mathrm{d}V$	$\frac{M_b E_m^{-2}}{\exp(\alpha_m t)}\iint_{S_b}\left\langle \tilde{\boldsymbol{u}}^i\cdot\hat{\boldsymbol{u}}\right\rangle \mathrm{d}S$	$-\frac{1}{2}M_b E_m^{-2}\iint_{S_b}\hat{\boldsymbol{u}}_m\cdot\hat{\boldsymbol{u}}_m\,\mathrm{d}S$
α_5	$\frac{E_m^{-2}}{\exp(2\alpha_m t)}\iiint_V \left\langle -\tilde{\boldsymbol{u}}\cdot\nabla\hat{p}\right\rangle \mathrm{d}V$	$\frac{-E_m^{-2}}{\exp(2\alpha_m t)}\iint_S\left\langle \boldsymbol{n}\cdot(\tilde{\boldsymbol{u}}\hat{p})\right\rangle \mathrm{d}S$	$\frac{1}{2}M_b E_m^{-2}\iint_{S_b}\hat{p}_m^2\,\mathrm{d}S$
α_6	$\frac{E_m^{-2}}{\exp(2\alpha_m t)}\iiint_V \left\langle M_b\tilde{\boldsymbol{u}}\cdot(\boldsymbol{U}\times\boldsymbol{\omega})\right\rangle \mathrm{d}V$	$\frac{-M_b E_m^{-2}}{\exp(2\alpha_m t)}\iint_S\left\langle \boldsymbol{n}\cdot\boldsymbol{U}\left(\frac{1}{2}\tilde{\boldsymbol{u}}\cdot\tilde{\boldsymbol{u}}\right)\right\rangle \mathrm{d}S$	$\frac{1}{4}k_m^{-2}M_b E_m^{-2}\iint_{S_b}(\nabla\hat{p}_m)^2\,\mathrm{d}S$
α_7	$\frac{E_m^{-2}}{\exp(2\alpha_m t)}\iiint_V \left\langle -\delta^2(\hat{\boldsymbol{u}}+\tilde{\boldsymbol{u}})\cdot(\nabla\times\boldsymbol{\omega})\right\rangle \mathrm{d}V$	$-\frac{\delta^2 E_m^{-2}k_m^2 M_b^{-2}}{2\exp(2\alpha_m t)}\iint_S\left\langle \tilde{\boldsymbol{u}}^2\right\rangle\Big\vert_{r=1}\mathrm{d}S$	$-\frac{1}{4}\delta^2 E_m^{-2}M_b^{-2}\iint_{S_b}(\nabla\hat{p}_m)^2\,\mathrm{d}S$
α_8	$\frac{E_m^{-2}}{\exp(2\alpha_m t)}\iiint_V \left\langle -\hat{\boldsymbol{u}}\cdot\nabla\tilde{p}\right\rangle \mathrm{d}V$	$\frac{2}{5}M_b^3 l^2/m^2$	$\frac{2}{5}M_b^3 l^2/m^2$
α_9	$\frac{-E_m^{-2}}{\exp(2\alpha_m t)}\iiint_V \left\langle \tilde{\boldsymbol{u}}\cdot\nabla\tilde{p}\right\rangle \mathrm{d}V$	$\frac{-E_m^{-2}}{\exp(2\alpha_m t)}\iint_S\left\langle \boldsymbol{n}\cdot\tilde{\boldsymbol{u}}\tilde{p}\right\rangle \mathrm{d}S$	$\frac{-1}{2}E_m^{-2}\iint_{S_N}\left[\tilde{u}_m^r\tilde{p}_m^r + \tilde{u}_m^i\tilde{p}_m^i\right]\mathrm{d}S$
α_{10}	$\frac{-E_m^{-2}}{\exp(2\alpha_m t)}\iiint_V \left\langle M_b(\hat{\boldsymbol{u}}+\tilde{\boldsymbol{u}})\cdot\nabla(\boldsymbol{U}\cdot\tilde{\boldsymbol{u}})\right\rangle \mathrm{d}V$	$\frac{-M_b E_m^{-2}}{\exp(2\alpha_m t)}\iint_S\left\langle \hat{\boldsymbol{n}}\cdot\left[\tilde{\boldsymbol{u}}(\boldsymbol{U}\cdot\tilde{\boldsymbol{u}})\right]\right\rangle \mathrm{d}S$	$\frac{-M_b}{2E_m^2}\iint_{S_N}\left[\left(\tilde{u}_m^i\right)^2 + \left(\tilde{u}_m^r\right)^2\right]U_z\mathrm{d}S$

Verification of these newly generated surface integrals is attempted with the use of the conventional circular port and slab motor geometries. Both asymptotic and numerical evaluations are presented. Asymptotic techniques are utilized for their ability to add deep insight into the underlying physics of a phenomenon, along with providing an approximate analytical form that greatly reduces calculations. The need for greater physical understanding will be demonstrated to be essential during this validation process. The two benchmark cases are chosen because of their extensive use in both experimental and numerical modeling of rocket combustion stability. The circular port motor is currently employed by Blomshield[6-10] at the Naval Air Warfare Center (NAWC) in combustion stability related studies. Researchers such as Apte and Yang,[11,12] Casalis *et al*.,[13-16] Liou *et al*.,[17-19]and Vuillot *et al*.[20-25] are making use of the slab (opposed plane) shape. This study will employ the nomenclature from previous work covering the internal burning cylinder[2,3,26,27] and slab motor,[1,28-30] respectively Figure 1 illustrates the attendant geometry.

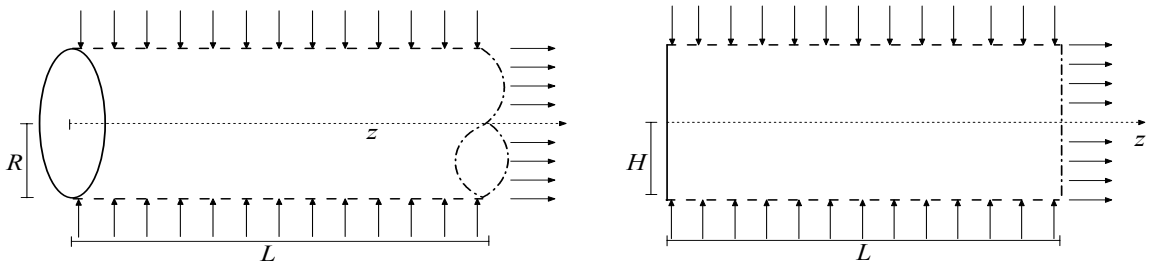

a) internal burning cylinder **b)** slab

Figure 1. Model solid rocket motors and coordinate systems.[3]

II. Cylindrical Configuration

A. Surface Integral Evaluation

Due to the simplicity of the recently derived surface integrals their evaluation is straightforward,[5] especially for the internal burning cylinder. Starting with the final integral expression for pressure coupling, one has

$$\alpha_1 = \tfrac{1}{2} M_b E_m^{-2} \iint_{S_b} \hat{p}_m^2 \left[A_b^{(r)} + 1 \right] \mathrm{d}S - \tfrac{1}{2} M_b E_m^{-2} \iint_{S_N} \hat{p}_m^2 \left[A_N^{(r)} + U_N \right] \mathrm{d}S \tag{1}$$

The two integrals can be expressed as

$$\alpha_1 = \tfrac{1}{2} M_b E_m^{-2} \int_0^l \int_0^{2\pi} \cos(k_m z)^2 \left[A_b^{(r)} + 1 \right] r \mathrm{d}\theta \, \mathrm{d}z \Big|_{r=1} - \tfrac{1}{2} M_b E_m^{-2} \int_0^1 \int_0^{2\pi} \cos(k_m z)^2 \left[A_N^{(r)} + U_N \right] r \mathrm{d}\theta \, \mathrm{d}r \Big|_{z=l} \tag{2}$$

Performing the prescribed integration leads to

$$\alpha_1 = \tfrac{4}{5} M_b \left[A_b^{(r)} - \gamma \right] \tag{3}$$

Similarly, from Table 1 the dilatational energy correction can be evaluated as

$$\alpha_2 = -\tfrac{2}{3} \delta^2 k_m E_m^{-2} \left[\int_0^l \int_0^{2\pi} M_b A_b^{(r)} \cos\left(\mathrm{k_m} z\right)^2 r \mathrm{d}\theta \, \mathrm{dz} \Big|_{r=1} - \int_0^1 \int_0^{2\pi} M_b A_N^{(r)} \cos\left(\mathrm{k_m} z\right)^2 r \mathrm{d}\theta \, \mathrm{dr} \Big|_{z=l} \right] - \tfrac{1}{3} \delta^2 E_m^{-2} k_m^2 \tag{4}$$

Further integration begets

$$\alpha_2 = -\tfrac{8}{15} \xi M_b^3 - \tfrac{16}{15} \xi M_b^4 k_m^{-1} \left(A_b^r - \gamma - 1 \right) \tag{5}$$

Given that $\alpha_3 = 0$, we continue to the *flow-turning* correction. Using the defined flowfield variables,[2,5,31] the integral form of α_4 becomes

$$\alpha_4 = \tfrac{1}{2} M_b E_m^{-2} \int_0^l \int_0^{2\pi} -\sin\left(x\right) exp\left(\phi\right) \sin\left(k_m z\right) \cos\left(\psi\right) \sin\left[\sin\left(\mathrm{x}\right) k_m z \right] r \mathrm{d}\theta \, \mathrm{dz} \Big|_{r=1} \tag{6}$$

At first glance, the above formulation appears quite daunting. However, by noting that at $r = 1$ many of the terms on the right-hand-side of Eq. (6) reduce to unity because $\sin\left[x(1)\right] = 1$, $exp\left[\phi(1)\right] = 1$, and $\cos\left[\psi\left(1\right)\right] = 1$; the integrand is simplified to the extent of yielding

$$\alpha_4 = -\tfrac{4}{5} M_b \tag{7}$$

It has been alluded to in previous studies[3,26] that the *rotational flow correction* and *flow-turning* terms are equal and opposite for a full length grain. This can be confirmed here; starting with

$$\alpha_5 = \tfrac{1}{2} E_m^{-2} \iint_{S_b} M_b \hat{p}_m^2 \, \mathrm{d}S \tag{8}$$

The integral for a circular port motor becomes

$$\alpha_5 = \tfrac{1}{2} E_m^{-2} M_b \int_0^l \int_0^{2\pi} \cos\left(k_m z\right)^2 r \, \mathrm{d}\theta \, \mathrm{dz} \Big|_{r=1} \tag{9}$$

Subsequent evaluation delivers

$$\alpha_5 = \tfrac{4}{5} M_b \tag{10}$$

The exact correspondence between the final versions of α_4 and α_5, for a full length grain, confirms the earlier insinuations to that effect.[3,26]

Using similar arguments, the mean vortical correction simplifies to

$$\alpha_6 = \tfrac{1}{4} k_m^{-2} E_m^{-2} \iint_{S_b} M_b \left(\nabla \hat{p}_m\right)^2 \mathrm{d}S \tag{11}$$

Applying the expression for the gradient of the pressure term gives

$$\alpha_6 = \tfrac{1}{4} E_m^{-2} M_b \int_0^l \int_0^{2\pi} \sin\left(k_m z\right)^2 r \,\mathrm{d}\theta \, dz\Big|_{r=1} \tag{12}$$

And so, evaluation of the double integral reads

$$\alpha_6 = \tfrac{2}{5} M_b \tag{13}$$

As we move on to consider α_7, we note that during the lengthy conversion of this viscous correction, we were forced to utilize the Von Kàrmàn-Polhausen method.[5] This method is applied using the assumption that, within the boundary layer, the length scales are such that a flat plate model may be utilized. This requires that a correction factor of two-thirds be applied when the surface integral is to be evaluated for a circular port motor. This is done to compensate for the lack of curvature in the flat plate model.[32] At the outset the surface form of α_7 becomes

$$\alpha_7 = -\tfrac{1}{6} \delta^2 E_m^{-2} M_b^{-2} \iint_{S_b} \left(\nabla \hat{p}_m\right)^2 \mathrm{d}S \tag{14}$$

Upon substitution of the pressure, one gets

$$\alpha_7 = -\tfrac{1}{6} \delta^2 E_m^{-2} M_b^{-2} \int_0^l \int_0^{2\pi} \sin\left(k_m z\right)^2 r \mathrm{d}\theta \mathrm{d}\, z\Big|_{r=1} \tag{15}$$

and so

$$\alpha_7 = -\tfrac{4}{15} \xi M_b \tag{16}$$

Owing to the fact that α_8 is $O(M_b^3)$, it is evaluated for a circular port motor using asymptotics; one obtains

$$\alpha_8 = \frac{2 M_b^3 l^2}{5 m^2} \left[1 - 3\xi^2 \frac{M_b^2 l^2}{(m\pi)^2} \right] << O(1) \tag{17}$$

Moving on to α_9 and α_{10}, we start with

$$\alpha_9 = -\tfrac{1}{2} E_m^{-2} \iint_{S_N} \left(\tilde{u}_m^r \tilde{p}_m^r + \tilde{u}_m^i \tilde{p}_m^i \right) \mathrm{d}S \tag{18}$$

and

$$\alpha_{10} = -\tfrac{1}{2} M_b E_m^{-2} \iint_{S_N} \left\{ \left[\tilde{u}_m^r \right]^2 + \left[\tilde{u}_m^i \right]^2 \right\} U_z \,\mathrm{d}S \tag{19}$$

One may substitute the circular port flowfield expressions[2,5,31] to get

$$\alpha_9 = -\tfrac{1}{4} \pi E_m^{-2} M_b \iint_{S_N} \begin{bmatrix} -\sin\left(x\right) \sin\left(2x\right) \sin\left(\psi\right)^2 exp\left(2\phi\right) \sin\left[\sin\left(x\right) k_m z \right]^2 z \\ -\sin(x) \sin\left(2x\right) \cos\left(\psi\right)^2 exp\left(2\phi\right) \sin\left[\sin\left(x\right) k_m z \right]^2 z \end{bmatrix} \mathrm{d}S \tag{20}$$

and

$$\alpha_{10} = -\tfrac{1}{2} \pi E_m^{-2} M_b \iint_{S_N} \begin{bmatrix} \sin\left(x\right)^2 \cos\left(x\right) \sin\left(\psi\right)^2 exp\left(2\phi\right) \sin\left[\sin\left(x\right) k_m z \right]^2 z \\ \sin\left(x\right)^2 \cos\left(x\right) \cos\left(\psi\right)^2 exp\left(2\phi\right) \sin\left[\sin\left(x\right) k_m z \right]^2 z \end{bmatrix} \mathrm{d}S \tag{21}$$

Making use of $\sin\left(2x\right) = 2\cos\left(x\right)\sin\left(x\right)$ and $\sin\left(\psi\right)^2 + \cos\left(\psi\right)^2 = 1$, we obtain

$$\alpha_9 = \tfrac{1}{2} \pi E_m^{-2} M_b \int_0^1 \int_0^{2\pi} \left[\sin\left(x\right) \sin\left(2x\right) exp\left(2\phi\right) \sin\left[\sin\left(x\right) k_m z \right]^2 z \right] r \mathrm{d}\theta \,\mathrm{d}r\Big|_{z=l} \tag{22}$$

and

$$\alpha_{10} = -\tfrac{1}{2} \pi E_m^{-2} M_b \int_0^1 \int_0^{2\pi} \left[\sin\left(x\right) \sin\left(2x\right) exp\left(2\phi\right) \sin\left[\sin\left(x\right) k_m z \right]^2 z \right] r \mathrm{d}\theta \,\mathrm{d}r\Big|_{z=l} \tag{23}$$

Clearly, when evaluated for a full-length circular port motor, $\alpha_9 + \alpha_{10} = 0$. In previous work[2] an integrand matching that of α_9 and α_{10} has been evaluated using asymptotics and verified numerically. The same can be applied here such that

$$\alpha_9 = \tfrac{5}{6}\pi^2 l M_b E_m^{-2} \left\{ [\pi^2 + 4(\xi + \sqrt{2})^2]^{-1} - \tfrac{1}{500} \right\} \tag{24}$$

and

$$\alpha_{10} = -\tfrac{5}{6}\pi^2 l M_b E_m^{-2} \left\{ [\pi^2 + 4(\xi + \sqrt{2})^2]^{-1} - \tfrac{1}{500} \right\} \tag{25}$$

The newly evaluated growth rate factors are logged and compared to those stemming from previous studies in Table 2. The individual factors display a strong correlation between volume and surface form. The discrepancy in α_2 is due to the volume form being unable to account for the admittance function at the propellant surface. These terms, being of $O(M_b^4)$, have no appreciable bearing on the results. It should be mentioned that the governing equations employed are only valid to $O(M_b)$; evidently, terms of $O(M_b^2)$ are ignored for the sake of consistency. As shown in Table 2, the *flow-turning* and *boundary layer pumping* are found identical to their volume forms at leading order. Similarly, α_1 and α_6 show exact agreement. Majdalani and coworkers[2] have shown that the asymptotic expressions for of α_9 and α_{10} are identical but opposite in sign. This is confirmed by the current work.

B. Numerical Comparison

Numerical integration of the surface integrals was performed for a group of representative motor geometry and propellant features. Three cardinal cases were selected as characteristic examples for testing combustion instability.[3] These representative motors are employed because they aptly characterize a wide spectrum of motors. Table 3 summarizes their physical parameters. The dimensional growth rates for the representative motors are calculated using Mathematica and posted in Table 4. The dimensionless growth rates represented in Table 2 are made dimensional via $\alpha^* = \alpha a_0 / R$. The acoustic mean flow correction, α_3, is skipped knowing its exact value of zero. It should be mentioned that a similar numerical study has been recently performed[2] in which the original volume integrals are evaluated for a circular port motor and the same cardinal cases described in Table 3. Results of those volume integrals can be compared to the ones obtained here in an effort to validate the integral conversions. Systemic verification is certainly helpful and represents an essential component of the scientific method. To that end, numerical data from volume integration is displayed in Table 4. A simple comparison suggests that values displayed in Table 4 are concurrent.

One point of discrepancy stems from the evaluation of the viscous correction, α_7, for the small motor (where an error of 33% is incurred). This relatively large error can be attributed to the small motor having a viscous parameter in excess of unity. This is also confirmed by comparing the asymptotic forms of α_7 in Table 2. At leading order the two expressions are identical, but we see that there exist additional ξ corrections in the volume form which are a result of a small ξ assumption during the analysis. The fact that the two forms compare so well at leading order intuitively denotes that the surface form will have the same limitation in ξ as the asymptotic volume form. This helps to bracket the practical range of applicability for the asymptotic solutions, specifically, to motors with $\xi < 1$.

The other eight growth rate integrals display a maximum percent error of 8.44%, which occurs in α_6 for the Reusable Solid Rocket Motor (RSRM). The numerical and asymptotic levels of agreement between volume and surface integral forms are gratifying and lend support to the current methodology. Flowfield variables can be difficult to calculate throughout the motor chamber. The surface forms mitigate this problem by offering integrals that are more easily amenable to evaluation and implementation into the SSP code.

Numerical evaluation of the surface integrals is performed via the most recent incarnation of the SSP code. This code makes use of the growth rate factors that are of $O(M_b)$ or larger. As such, α_2, α_3 and α_8 are not evaluated. Also, α_9 and α_{10} are not programmed in SSP because they have been shown to cancel. Forthwith, the SSP results are presented in Table 7. Note that they are nearly identical to the numerically evaluated surface integrals given in Table 4.

Table 2. Asymptotic approximations of rotational stability integrals in cylindrical geometry.

	Rotational set in surface form	Asymptotic volume form	Asymptotic surface form
E_m^2	$E_m^2 = \frac{1}{2}\iiint[(\hat{p}_m)^2 + \hat{\boldsymbol{u}}_m \cdot \hat{\boldsymbol{u}}_m + 2\hat{\boldsymbol{u}}_m \cdot \tilde{\boldsymbol{u}}_m^i + \tilde{\boldsymbol{u}}_m^r \cdot \tilde{\boldsymbol{u}}_m^r + \tilde{\boldsymbol{u}}_m^i \cdot \tilde{\boldsymbol{u}}_m^i]\mathrm{d}V$		
α_1	$\frac{-E_m^{-2}}{\exp(2\alpha_m t)}\iint_s \left\langle \boldsymbol{n}\cdot\left[\hat{p}\hat{\boldsymbol{u}} + \frac{1}{2}M_b\boldsymbol{U}(\hat{p})^2\right] - M_b\left[\boldsymbol{n}\cdot\hat{\boldsymbol{u}}(\boldsymbol{U}\cdot\hat{\boldsymbol{u}})\right]\right\rangle \mathrm{d}S$	$\frac{4}{5}M_b\left[A_b^{(r)} - \gamma\right]$	$\frac{4}{5}M_b\left[A_b^{(r)} - \gamma\right]$
α_2	$\frac{4k_m\delta^2E_m^{-2}}{3\exp(2\alpha_m t)}\iint_S \left\langle \boldsymbol{n}\cdot(\hat{p}\hat{\boldsymbol{u}})\right\rangle \mathrm{d}S - \frac{1}{3}\delta^2E_m^{-2}k_m^2\pi l$	$-\frac{8}{15}\xi M_b^3$	$-\frac{8}{15}\xi M_b^3 + O\left(M_b^4\right)$
α_3	0	0	0
α_4	$\frac{M_bE_m^{-2}}{\exp(\alpha_m t)}\iint_{S_b}\left\langle \tilde{\boldsymbol{u}}^i\cdot\hat{\boldsymbol{u}}\right\rangle \mathrm{d}S$	$-\frac{4}{5}M_b\left(1-\pi^{-2}M_b^2\xi^2l^2\right)$	$-\frac{4}{5}M_b$
α_5	$\frac{-E_m^{-2}}{\exp(2\alpha_m t)}\iint_S\left\langle \boldsymbol{n}\cdot(\tilde{\boldsymbol{u}}\hat{p})\right\rangle \mathrm{d}S$	$\frac{4}{5}M_b\left(1-\pi^{-2}M_b^2\xi^2l^2\right)$	$\frac{4}{5}M_b$
α_6	$\frac{-M_bE_m^{-2}}{\exp(2\alpha_m t)}\iint_S\left\langle \boldsymbol{n}\cdot\boldsymbol{U}\left(\frac{1}{2}\tilde{\boldsymbol{u}}\cdot\tilde{\boldsymbol{u}}\right)\right\rangle \mathrm{d}S$	$\frac{2}{5}M_b$	$\frac{2}{5}M_b$
α_7	$-\frac{\delta^2E_m^{-2}k_m^2M_b^{-2}}{2\exp(2\alpha_m t)}\iint_S\left\langle \tilde{\boldsymbol{u}}^2\right\rangle\Big\vert_{r=1}\mathrm{d}S$	$-\frac{4}{15}M_b\xi\left(1-\frac{1}{2}\xi + O\left(\xi^2\right)\right)$	$-\frac{4}{15}\xi M_b$
α_8	$\frac{2}{5}M_b^3l^2/m^2$	$\frac{2}{5}M_b^3l^2/m^2$	$\frac{2}{5}M_b^3l^2/m^2$
α_9	$\frac{-E_m^{-2}}{\exp(2\alpha_m t)}\iint_S\left\langle \boldsymbol{n}\cdot\tilde{\boldsymbol{u}}\tilde{p}\right\rangle \mathrm{d}S$	$\frac{5}{6}\pi^2lM_bE_m^{-2}\left\{[4(\xi+\sqrt{2})^2]^{-1} + \pi^2 - \frac{1}{500}\right\}$	$\frac{5}{6}\pi^2lM_bE_m^{-2}\left\{[4(\xi+\sqrt{2})^2]^{-1} + \pi^2 - \frac{1}{500}\right\}$
α_{10}	$\frac{-M_bE_m^{-2}}{\exp(2\alpha_m t)}\iint_S\left\langle \hat{\boldsymbol{n}}\cdot\left[\tilde{\boldsymbol{u}}(\boldsymbol{U}\cdot\tilde{\boldsymbol{u}})\right]\right\rangle \mathrm{d}S$	$\frac{-5}{6}\pi^2lM_bE_m^{-2}\left\{[4(\xi+\sqrt{2})^2]^{-1} + \pi^2 - \frac{1}{500}\right\}$	$\frac{-5}{6}\pi^2lM_bE_m^{-2}\left\{[4(\xi+\sqrt{2})^2]^{-1} + \pi^2 - \frac{1}{500}\right\}$

Table 3. Physical parameters for the routinely cited baseline cases[3]

Motor	α_{10} (m)	R (m)	M_b	δ	k_m	S	ξ	f (Hz)	$A_b^{(r)}$	(m/s)
Small Motor	0.60	0.025	1.7^{-3}	5.49^{-4}	1.31^{-1}	77.00	1.0512	1227	2.5	1472
Tactical Rocket	2.03	0.102	3.1^{-3}	2.74^{-4}	1.58^{-1}	50.92	0.0628	360	1.2	1462
RSRM	35.1	0.700	2.3^{-3}	1.04^{-4}	6.27^{-2}	27.24	0.0035	19.5	1.0	1369

Table 4. Numerically evaluated surface (S) and volume (V) integrals of individual growth rates (sec^{-1})[2]

	study	α_1^*	α_2^*	α_4^*	α_5^*	α_6^*	α_7^*	α_8^*	α_9^*
otor	S	96.1	-1.62^{-4}	-80.1	80.1	40.0	-28.06	0.0644	11.5
	V	96.1	-1.62^{-4}	-80.0	80.0	39.2	-18.61	0.0644	11.5
Rocket	S	-3.55	-1.43^{-5}	-35.5	35.5	17.8	-0.744	0.0627	9.62
	V	-3.55	-1.43^{-5}	-35.7	35.7	16.5	-0.716	0.0627	9.62
	S	-1.08	-4.43^{-8}	-3.60	3.60	1.80	-0.00419	0.0179	1.01
	V	-1.08	-4.43^{-8}	-3.66	3.66	1.66	-0.00411	0.0179	1.01

Table 5. SSP evaluated surface integrals of individual growth rates (sec^{-1})

Motor	α_1^*	α_4^*	α_5^*	α_6^*	α_7^*
Motor	96.41	-80.01	80.01	40.04	-28.0
l Rocket	-3.520	-35.54	35.54	17.78	-0.74
Shuttle SRB	-1.080	-3.600	3.600	1.800	-0.004

III. Slab Configuration

A. Surface Integral Evaluation

We begin by outlining the evaluation process along similar lines to those followed in the previous section. We first consider

$$\alpha_1 = \tfrac{1}{2} M_b E_m^{-2} \iint_{S_b} \hat{p}_m^2 \left[A_b^{(r)} + 1 \right] \mathrm{d}S - \tfrac{1}{2} M_b E_m^{-2} \iint_{S_N} \hat{p}_m^2 \left[A_N^{(r)} + U_N \right] \mathrm{d}S \tag{26}$$

which can be expressed as

$$\alpha_1 = M_b E_m^{-2} \int_0^w \int_0^l \cos(k_m z)^2 \left[A_b^{(r)} + 1 \right] \mathrm{d}z \, \mathrm{d}x \; - M_b E_m^{-2} \int_0^l \int_0^w \cos(k_m z)^2 \left[A_N^{(r)} + U_N \right] \mathrm{d}x \, \mathrm{d}y \Big|_{z=l} \tag{27}$$

Evaluating the given integration results in

$$\alpha_1 = \tfrac{4}{9} M_b \left[A_b^{(r)} + 1 - 2\gamma \right] \tag{28}$$

Next, the dilatational energy correction can be evaluated from

$$\alpha_2 = -\tfrac{4}{3} \delta^2 k_m E_m^{-2} \left[\int_0^l \int_0^w M_b A_b^{(r)} \cos\left(\mathrm{k_m} z\right)^2 \mathrm{dx dz} - \int_0^1 \int_0^w M_b A_N^{(r)} \cos\left(\mathrm{k_m} z\right)^2 r \mathrm{dx} \, \mathrm{dy} \Big|_{z=l} \right] - \tfrac{2}{3} \delta^2 E_m^{-2} k_m^2 \, lw \tag{29}$$

Integration leads to

$$\alpha_2 = -\tfrac{16}{27} \xi M_b^3 + \tfrac{32}{27} \xi M_b^4 \, l / \pi \left(\tfrac{1}{2} A_b^r + \gamma - 1 \right) \tag{30}$$

Continuing to the *flow-turning* correction, we use the defined flowfield variables to extract

$$\alpha_4 = \tfrac{1}{2} M_b E_m^{-2} \int_0^l \int_0^{2\pi} -\sin\left(x\right) exp\left(\phi\right) \sin\left(k_m z\right) \cos\left(\psi\right) \sin\left[\sin\left(\mathrm{x}\right) k_m z \right] r \mathrm{d}\theta \, \mathrm{dz} \Big|_{r=1} \tag{31}$$

Note that at $y = 1$ many of the terms on the right-hand-side of Eq. (31) reduce to unity because $\cos\left[\eta(0)\right] = 1$, $exp\left[\phi(0)\right] = 1$, and $\cos\left[\psi\left(0\right)\right] = 1$; the integrand yields

$$\alpha_4 = -\tfrac{4}{9} M_b \tag{32}$$

Continuing on to α_5, we have

$$\alpha_5 = \tfrac{1}{2} E_m^{-2} \iint_{S_b} M_b \hat{p}_m^2 \, \mathrm{d}S \tag{33}$$

The integral for a slab motor becomes

$$\alpha_5 = E_m^{-2} M_b \int_0^w \int_0^l \cos\left(k_m z\right)^2 \mathrm{dz dx} \tag{34}$$

Subsequent evaluation gives

$$\alpha_5 = \tfrac{4}{9} M_b \tag{35}$$

Using similar arguments, the mean vortical correction simplifies to

$$\alpha_6 = \tfrac{1}{4} k_m^{-2} E_m^{-2} \iint_{S_b} M_b \left(\nabla \hat{p}_m \right)^2 \mathrm{d}S \tag{36}$$

Applying the expression for the gradient of the pressure term yields

$$\alpha_6 = \tfrac{1}{2} E_m^{-2} M_b \int_0^w \int_0^l \sin\left(k_m z\right)^2 \mathrm{d}z\mathrm{d}x \tag{37}$$

And so, evaluation of the double integral reads

$$\alpha_6 = \tfrac{2}{9} M_b \tag{38}$$

As we move on to consider α_7, we realize that the outset the surface form becomes, as usual

$$\alpha_7 = -\tfrac{1}{4} \delta^2 E_m^{-2} M_b^{-2} \iint_{S_b} \left(\nabla \hat{p}_m\right)^2 \mathrm{d}S \tag{39}$$

Upon substitution of the pressure, one gets

$$\alpha_7 = -\tfrac{1}{2} \delta^2 E_m^{-2} M_b^{-2} \int_0^w \int_0^l \sin\left(k_m z\right)^2 \mathrm{d}z\mathrm{d}x \tag{40}$$

and so

$$\alpha_7 = -\tfrac{2}{9} \xi M_b \tag{41}$$

Owing to the fact that α_8 is $O(M_b^3)$, this term can be evaluated for a slab motor using asymptotics; one obtains

$$\alpha_8 = -\tfrac{1}{18} \pi^2 M_b^3 \left(\xi^2 M_b^2 - m^2 \pi^2 l^{-2}\right)\left(\xi^2 M_b^2 + m^2 \pi^2 l^{-2}\right)^{-2} << O(1) \tag{42}$$

Moving on to α_9 and α_{10}, we start with

$$\alpha_9 = -\tfrac{1}{2} E_m^{-2} \iint_{S_N} \left(\tilde{u}_m^r \tilde{p}_m^r + \tilde{u}_m^i \tilde{p}_m^i\right) \mathrm{d}S \tag{43}$$

and substitute $\tilde{p}_m^i$ and $\tilde{p}_m^r$, such that

$$\alpha_{10} = -\tfrac{1}{2} M_b E_m^{-2} \iint_{S_N} \left\{\left[\tilde{u}_m^r\right]^2 + \left[\tilde{u}_m^i\right]^2\right\} U_z \, \mathrm{d}S \tag{44}$$

After employing the needed flowfield variables,[1] one arrives at

$$\alpha_9 = -\tfrac{1}{4} \pi E_m^{-2} M_b \iint_{S_N} \begin{bmatrix} -\cos\left(\eta\right)^2 \sin\left(\eta\right) \sin\left(\psi\right)^2 exp\left(2\phi\right) \sin\left[\cos\left(\eta\right) k_m z\right]^2 z \\ -\cos\left(\eta\right)^2 \sin\left(\eta\right) \cos\left(\psi\right)^2 exp\left(2\phi\right) \sin\left[\cos\left(\eta\right) k_m z\right]^2 z \end{bmatrix} \mathrm{d}S \tag{45}$$

and

$$\alpha_{10} = -\tfrac{1}{4} \pi E_m^{-2} M_b \iint_{S_N} \begin{bmatrix} \cos\left(\eta\right)^2 \sin\left(\eta\right) \sin\left(\psi\right)^2 exp\left(2\phi\right) \sin\left[\cos\left(\eta\right) k_m z\right]^2 z \\ \cos\left(\eta\right)^2 \sin\left(\eta\right) \cos\left(\psi\right)^2 exp\left(2\phi\right) \sin\left[\cos\left(\eta\right) k_m z\right]^2 z \end{bmatrix} \mathrm{d}S \tag{46}$$

These result in

$$\alpha_9 = \tfrac{1}{2} \pi E_m^{-2} M_b \int_0^w \int_0^1 \left[\sin\left(\eta\right) \cos\left(\eta\right)^2 exp\left(2\phi\right) \sin\left[\cos\left(\eta\right) k_m z\right]^2 z\right] \mathrm{d}y \, \mathrm{d}x\big|_{z=l} \tag{47}$$

and

$$\alpha_{10} = -\tfrac{1}{2} \pi E_m^{-2} M_b \int_0^w \int_0^1 \left[\cos\left(\eta\right)^2 \sin\left(\eta\right) exp\left(2\phi\right) \sin\left[\cos\left(\eta\right) k_m z\right]^2 z\right] \mathrm{d}y \, \mathrm{d}x\big|_{z=l} \tag{48}$$

Clearly, when evaluated for a full-length slab motor, $\alpha_9 + \alpha_{10} = 0$. In previous work[1] an integrand matching that of α_9 and α_{10} was evaluated using asymptotics and verified numerically. The same can be applied here such that

$$\alpha_9 = \tfrac{4}{27} M_b \left(1 - \tfrac{3}{2} \pi^{-2}\right)\left(\tfrac{427}{425} + \tfrac{917}{374} \xi + \tfrac{95}{61} \xi^2 + \tfrac{437}{670} \xi^3 + \tfrac{101}{847} \xi^4 + \tfrac{1}{65} \xi^5 + \tfrac{1}{794} \xi^6\right)^{-1} \tag{49}$$

and

$$\alpha_9 = -\tfrac{4}{27} M_b \left(1 - \tfrac{3}{2} \pi^{-2}\right)\left(\tfrac{427}{425} + \tfrac{917}{374} \xi + \tfrac{95}{61} \xi^2 + \tfrac{437}{670} \xi^3 + \tfrac{101}{847} \xi^4 + \tfrac{1}{65} \xi^5 + \tfrac{1}{794} \xi^6\right)^{-1} \tag{50}$$

Table 6 displays the asymptotic growth rate factors achieved from the surface forms along with those derived in a previous study directly from volume integrals.[1] Many similarities are seen between the slab and circular port motor cases. For instance α_1 shows exact agreement between surface and volume forms. Also, the asymptotic values concur at leading order for α_2, α_4, α_5 and α_6. The discrepancy in α_2 is due to the volume form being unable to account for the admittance function at the propellant surface. The higher order terms in the volume form of α_4 and α_5 are of $O(M_b^2)$, which have been already stated as beyond the accuracy of the governing equations.

Table 6. Asymptotic approximations of rotational stability integrals in slab geometry

	Rotational set in surface form	Asymptotic volume form	Asymptotic surface form
E_m^2	$E_m^2 = \frac{1}{2}\iiint[(\hat{p}_m)^2 + \hat{\boldsymbol{u}}_m \cdot \hat{\boldsymbol{u}}_m + 2\hat{\boldsymbol{u}}_m \cdot \tilde{\boldsymbol{u}}_m^i + \tilde{\boldsymbol{u}}_m^r \cdot \tilde{\boldsymbol{u}}_m^r + \tilde{\boldsymbol{u}}_m^i \cdot \tilde{\boldsymbol{u}}_m^i]\mathrm{d}V$		
α_1	$\frac{-E_m^{-2}}{\exp(2\alpha_m t)}\iint_s \left\langle \boldsymbol{n}\cdot\left[\hat{p}\hat{\boldsymbol{u}} + \frac{1}{2}M_b\boldsymbol{U}(\hat{p})^2\right] - M_b\left[\boldsymbol{n}\cdot\hat{\boldsymbol{u}}(\boldsymbol{U}\cdot\hat{\boldsymbol{u}})\right]\right\rangle \mathrm{d}S$	$\frac{4}{9}M_b\left[\left(A_b^{(r)}+1\right) - 2\gamma\right]$	$\frac{4}{9}M_b\left[A_b^{(r)} + 1 - 2\gamma\right]$
α_2	$\frac{4k_m\delta^2 E_m^{-2}}{3\exp(2\alpha_m t)}\iint_S \left\langle \boldsymbol{n}\cdot(\hat{p}\hat{\boldsymbol{u}})\right\rangle \mathrm{d}S - \frac{1}{3}\delta^2 E_m^{-2}k_m^2\pi l$	$-\frac{16}{27}\xi M_b^3 << O(1)$	$-\frac{16}{27}\xi M_b^3 + O\left(M_b^4\right)$
α_3	0	0	0
α_4	$\frac{M_b E_m^{-2}}{\exp(\alpha_m t)}\iint_{S_b}\left\langle \tilde{\boldsymbol{u}}^i\cdot\hat{\boldsymbol{u}}\right\rangle \mathrm{d}S$	$-\frac{4}{9}M_b\left(1+\pi^{-2}M_b^2\xi^2 l^2 m^{-2}\right)^{-1}$	$-\frac{4}{9}M_b$
α_5	$\frac{-E_m^{-2}}{\exp(2\alpha_m t)}\iint_S \left\langle \boldsymbol{n}\cdot(\tilde{\boldsymbol{u}}\hat{p})\right\rangle \mathrm{d}S$	$\frac{4}{9}M_b\left(1+\pi^{-2}M_b^2\xi^2 l^2 m^{-2}\right)^{-1}$	$\frac{4}{9}M_b$
α_6	$\frac{-M_b E_m^{-2}}{\exp(2\alpha_m t)}\iint_S \left\langle \boldsymbol{n}\cdot\boldsymbol{U}\left(\frac{1}{2}\tilde{\boldsymbol{u}}\cdot\tilde{\boldsymbol{u}}\right)\right\rangle \mathrm{d}S$	$\frac{2}{9}M_b\{1-\frac{1}{24}\left[m\pi^2\xi^4 e^{2\xi}\left(\pi^2-12\right)\right]^{-1} \times\left[\frac{39}{85}+\frac{1}{82}\xi+\frac{7}{13}\exp\left(-\frac{107}{50}\xi\right)\right] \times\left(4m\pi^2+3\right)\left(12\xi^2\left(1+2\xi-e^{2\xi}\right)\right. \left.+\pi^2\left\{3e^{2\xi}-3-2\xi\left[3+\xi\left(3+2\xi\right)\right]\right\}\right)\}$	$\frac{2}{9}M_b$
α_7	$-\frac{\delta^2 E_m^{-2}k_m^2 M_b^{-2}}{2\exp(2\alpha_m t)}\iint_S \left\langle \tilde{\boldsymbol{u}}^2\right\rangle\Big\vert_{r=1}\mathrm{d}S$	$-\frac{1}{9}\pi^2\left(24m-\pi^2\right)^{-1}ml^{-2}\delta^2\xi^{-3}M_b^{-2} \times\left(3e^{-2\xi}\left\{16m\xi^2\left(e^{2\xi}-1\right)\right.\right. \left.\left.+\pi^2\left[1-e^{2\xi}+2\xi\left(1+\xi\right)\right]\right\}\right)$	$-\frac{2}{9}\xi M_b$
α_8	$\frac{2}{5}M_b^3 l^2/m^2$	$\frac{2}{5}M_b^3 l^2/m^2 << O(1)$	$\frac{2}{5}M_b^3 l^2/m^2$
α_9	$\frac{-E_m^{-2}}{\exp(2\alpha_m t)}\iint_S \left\langle \boldsymbol{n}\cdot\tilde{\boldsymbol{u}}\tilde{p}\right\rangle \mathrm{d}S$	$\frac{4}{27}M_b\left(1-\frac{3}{2}\pi^{-2}\right)\left(\frac{427}{425}+\frac{917}{374}\xi+\frac{95}{61}\xi^2 +\frac{437}{670}\xi^3+\frac{101}{847}\xi^4+\frac{1}{65}\xi^5+\frac{1}{794}\xi^6\right)^{-1}$	$\frac{4}{27}M_b\left(1-\frac{3}{2}\pi^{-2}\right)\left(\frac{427}{425}+\frac{917}{374}\xi+\frac{95}{61}\xi^2 +\frac{437}{670}\xi^3+\frac{101}{847}\xi^4+\frac{1}{65}\xi^5+\frac{1}{794}\xi^6\right)^{-1}$
α_{10}	$\frac{-M_b E_m^{-2}}{\exp(2\alpha_m t)}\iint_S \left\langle \hat{\boldsymbol{n}}\cdot\left[\tilde{\boldsymbol{u}}(\boldsymbol{U}\cdot\tilde{\boldsymbol{u}})\right]\right\rangle \mathrm{d}S$	$\frac{-4}{27}M_b\left(1-\frac{3}{2}\pi^{-2}\right)\left(\frac{427}{425}+\frac{917}{374}\xi+\frac{95}{61}\xi^2 +\frac{437}{670}\xi^3+\frac{101}{847}\xi^4+\frac{1}{65}\xi^5+\frac{1}{794}\xi^6\right)^{-1}$	$\frac{-4}{27}M_b\left(1-\frac{3}{2}\pi^{-2}\right)\left(\frac{427}{425}+\frac{917}{374}\xi+\frac{95}{61}\xi^2 +\frac{437}{670}\xi^3+\frac{101}{847}\xi^4+\frac{1}{65}\xi^5+\frac{1}{794}\xi^6\right)^{-1}$

Despite the daunting appearance of α_7 in its volume form, it can be shown that it matches the surface integral at leading order, with some higher order terms in ξ. This divergence is shared by α_6 and is investigated more thoroughly later. As expected, the asymptotic expressions for the α_9 and α_{10} terms are identical and opposite in sign.

B. Numerical Comparison

In much the same fashion as before integration of the surface integrals is performed numerically using a group of representative motors with comparable dimensions to the cardinal cases presented for the circular port motor.[3] Table 7 lists their physical parameters. In this case the dimensionless growth rates are made dimensional through multiplication by $\alpha^* = \alpha a_0/H$. It should be mentioned that a similar numerical study has been recently performed[1] in which the original volume integrals are evaluated for a slab rocket motor and the same cardinal cases described in Table 7. Results of those volume integrals can be compared to the ones obtained here in an effort to validate the newly generated surface integrals. The numerical values displayed in Table 8 show favorable agreement between the two integral forms.

Table 7. Physical parameters for the routinely cited baseline cases conveyed to the slab motor[3]

Motor	L (m)	H (m)	W (m)	M_b	δ	k_m	S	ξ	f (Hz)	$A_b^{(r)}$	a_0 (m/s)
Small Motor	0.60	0.025	0.200	1.7^{-3}	5.49^{-4}	1.31^{-1}	77.00	1.0512	1227	2.5	1472
Tactical Rocket	2.03	0.102	0.816	3.1^{-3}	2.74^{-4}	1.58^{-1}	50.92	0.0628	360	1.2	1462
Space Shuttle SRB	35.1	0.700	5.600	2.3^{-3}	1.04^{-4}	6.27^{-2}	27.24	0.0035	19.5	1.0	1369

The most obvious deviation between the volume and surface forms within the slab geometry appears in the two parameters, aside from *flow-turning*, that involve unsteady vorticity. The creation of unsteady vorticity at the chamber boundaries is an unavoidable result of satisfying the no slip condition. These terms are dubbed the mean vortical correction and the viscous correction (α_6 and α_7 respectively) for their physical interpretations.[3,4] Both terms are recent additions to the combustion instability community, being discovered when rotational terms were taken into account.[3] The most evident reason for these numerical discrepancies is the omission of sidewall effects. The slab rocket motor is defined with mass injection from the upper and lower boundaries along with inert vertical boundaries. With the unsteady vorticity being a main driver of these two terms it is important to account for the entire vorticity vector. Figure 2 displays the unsteady vorticity vectors for both the slab and cylindrical motor. For the slab motor the vectors along the sidewalls are displayed as dashed lines because this study does not integrate over the inert surfaces. Integrating solely over the burning surface will cause the vorticity vector to terminate at the

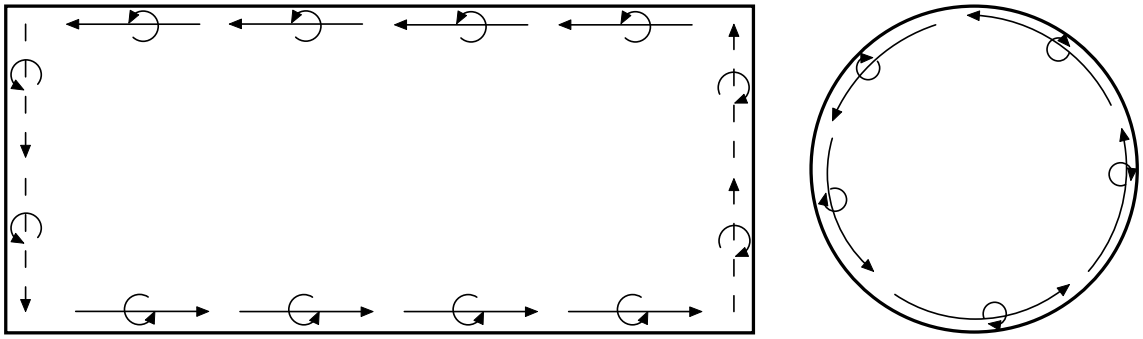

Figure 2. Vorticity vectors in slab and cylindrical motor.

sidewalls, which is, of course, unphysical. Figure 2 demonstrates that, for the circular port motor, integrating over the burning surface can accurately account for the unsteady vorticity created at the chamber boundaries. This may be why the volume and surface integrals show better compliance in the circular port motor case. Therefore it may be argued that the application of surface integrals to the burning surface alone is insufficient. We remark that when converting volume integrals into surface form it is essential that all boundaries be included. We thus realize that the conversion of α_6 and α_7 may be remiss by its exclusion of the lateral walls.

Besides physical reasoning this disagreement can be demonstrated with the use of asymptotics. Looking at the asymptotic expressions for α_6 we see that the volume and surface forms are identical at leading order. But, the volume integral has higher-order terms in ξ. Tracing the origin of these terms we see that they originate from the $\exp(\phi)$ function, more specifically when this function is integrated over the range of y. Note that $\phi = \phi(\xi, y)$. At the burning surface ($y = 0, 2$), $\exp(\phi)$ is equal to unity. This suggests that irrespective of the approximation used, the higher order terms of ξ are not involved during integration over the burning surface. The remedy lies, perhaps, in taking the sidewalls into account.

Although beyond the scope of this study, implementing sidewall effects may be accomplished with considerable effort. According to Table 1 the mean vortical correction involves the normal projection of the mean velocity vector. Initially one would assume that since the mean flow is zero at the inert sidewall it is not possible to evaluate this term. Yet, further scrutiny suggests that there is a velocity component normal to the sidewall which is induced by the impending boundary layer. Boundary layer displacement will impart a velocity normal to the sidewalls. This term, though small, is likely to be of $O(M_b)$, thus worthy of consideration. In analyzing α_7 we experience the same limitation in ξ affecting the small motor. This limitation, as seen in the cylindrical motor, produces a larger

Table 8. Numerically evaluated surface (S) and volume (V) integrals of individual growth rates $(sec^{-1})^2$

Motor	Study	α_1^*	α_2^*	α_4^*	α_5^*	α_6^*	α_7^*	α_8^*	α_9^*
otor	S	40.04	-1.73^{-4}	-44.49	44.49	22.24	-23.38	0.00925	2.02
	V	40.04	-1.80^{-4}	-44.37	44.37	19.37	-15.52	0.00925	2.02
Rocket	S	-7.89	-1.53^{-5}	-19.75	19.75	9.87	-0.620	0.00939	4.79
	V	-7.89	-1.59^{-5}	-19.75	19.75	6.62	-0.975	0.00939	4.79
	S	-1.20	-4.63^{-8}	-2.00	2.00	0.99	-0.00349	0.00332	0.56
	V	-1.20	-4.92^{-8}	-2.01	2.01	0.64	-0.00608	0.00332	0.56

value in the surface case. This trend is not observed in the other two motors, that exhibit $\xi < 1$. Again, utilizing the same rationale stated for α_6, the discrepancy in these cases is suspected to be a result of the inert sidewalls. Terms of higher order in ξ can only be obtained by integrating over y. Thus, in order to obtain convergence in α_7, one must quantify the dissipation of energy due to the boundary layer on the chamber's lateral boundaries.

It must be noted that during the conversion of α_6 and α_7 some assumptions that may only be valid for the cylindrical model were applied. Curvature effects could also play a role in the numerical discrepancies between volume and surface forms. To look at this problem from a different angle one may recognize that the main reason for the discrepancies in the Cartesian geometry is due to its infinite curvature. By comparison with the cylindrical motor, a slab exhibits a much larger penetration depth of rotational flow ingredients. It therefore inherits a stronger dependence on ξ. In a previous study by Majdalani,[33] ξ was shown to be the reciprocal of the penetration number $S_p = \rho V_b^3 / \omega^2 \mu R$, specifically, the key agent in control of the depth of penetration. The irrotational core in the slab is much thinner than in the cylinder. This can be said of both mean and unsteady flow components. The deeper penetration of the mean flow streamlines is illustrated, for example, in the lower half of Figure 3. The analogous wave dependence is described along similar lines by Majdalani and Roh.[34] The stronger dependence on ξ in the slab motor is evident in the cartesian expressions for α_6 and α_7 in Table 6. Conversely, the same integrals in Table 2 display weak sensitivity to ξ. This causes the latter to be in better agreement with the surface integral formulas

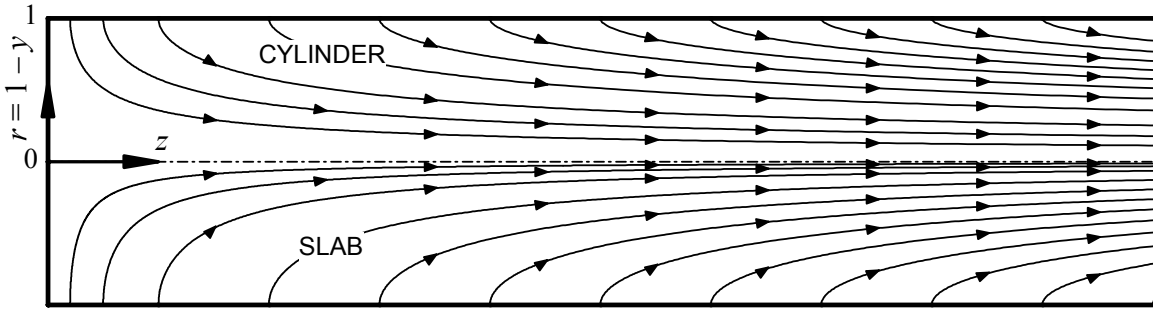

Figure 3. Streamline curvature for the cylindrical and slab motors.

which are independent of the core's sensitivity to the penetration number.

Despite the differences in numerical values these errors are within acceptable ranges. The SSP code is used to evaluate the surface integrals in order to augment the in house capabilities. The SSP results are presented in Table 9 where they are shown to nearly match the surface integral values presented in Table 8. The implementation of surface integrals in the SSP code is possible because the new surface forms are only functions of the local pressure and pressure gradients. This highlights the major achievement of the present study. Terms, which were before deemed too complex to evaluate, can now be calculated for an arbitrary shape handled by SSP.

IV. Conclusion

The current study validates a useful step forward in improving our modeling capabilities of acoustic instability growth for motors undergoing linear oscillations. It has been demonstrated that the newly generated surface integral form of the combustion stability growth rate terms successfully reproduces, within an acceptable range of error, the numerical values of the more complex volume form. It must be noted that these integrals correspond to the linear

Table 9. SSP evaluated surface integrals of slab individual growth rates (sec^{-1})

Motor	α_1^*	α_4^*	α_5^*	α_6^*
	40.23	-44.49	44.49	22.24
	-7.87	-19.75	19.75	9.87
	-1.20	-2.000	2.000	1.00

growth rate regime preceding the onset of nonlinear oscillations. From this standpoint, it may be seen that a key contribution of this study lies, perhaps, in its proof-of-concept role in converting the linear stability growth rates. Here they are shown to be amenable to surface transformation despite their relative complexity. The feasibility of this approach may be readily extended to other combustion instability mechanisms that are expressed in volume integral form. For instance this study does not attempt to convert the terms corresponding to particle damping, distributed combustion or velocity coupling.[35-43] These remain to be addressed or resolved as needed.

Another key aspect that this study addresses is the impact of retaining the pseudopressure which is often neglected in the literature. Being the unsteady pressure wave (or pseudosound) generated at solid boundaries, $\tilde{p}$ is ignored in stability assessments because of its small magnitude and its rapid decay away from the burning surface. However, considering that most important instability mechanisms occur in close vicinity to the propellant surface, it is not surprising that one of the two pseudo corrections is large (i.e., α_9).[4] This point is confirmed in the present analysis as pseudosound-related corrections are carefully examined in both volume and surface form. In later studies, it may be shown that α_9 and α_{10} can cancel each other's contribution for a general flowfield. The same can be said of *flow-turning* and other rotational flow corrections made manifest in recent work.

The updating of SSP via surface integrations should eliminate the need to evaluate the vortical flowfield over the chamber volume. This will not only simplify the evaluation of the stability integrals, but will greatly enhance the accuracy of SSP predictions. Subsequently, users of the code will only need to be concerned with providing accurate estimates of propellant properties and injection characteristics along the motor boundaries.

Current nonlinear combustion instability approaches have displayed strong dependency on the linear models. In fact, a nonlinear solution cannot be obtained without a full understanding of linear behavior. A recent study by Flandro *et al.* [44] has shown appreciable progress on this front.

Acknowledgments

This work was sponsored by the National Science Foundation through Grant No. CMS-0353518, Program Manager, Dr. Masayoshi Tomizuka. Grateful appreciation is expressed for additional University of Tennessee support derived from the Edward J. and Carolyn P. Boling Chair of Excellence in Advanced Propulsion, and the Jack D. Whitfield Professorship of High Speed Flows. The authors are deeply grateful to Dr. Fred S. Blomshield, Head of Combustion and Propulsion Research, Naval Air Warfare Center, for promoting research in combustion instability.

References

[1]Fischbach, S. R., Majdalani, J., and Flandro, G. A., "Acoustic Instability of the Slab Rocket Motor," AIAA Paper 2004-4061, July 2004.

[2]Majdalani, J., Flandro, G. A., and Fischbach, S. R., "Some Rotational Corrections to the Acoustic Energy Equation in Injection-Driven Enclosures," *Physics of Fluids*, 2005, p. in press.

[3]Flandro, G. A., and Majdalani, J., "Aeroacoustic Instability in Rockets," *AIAA Journal,* Vol. 41, No. 3, 2003, pp. 485-497.

[4]Chibli, H. A., Majdalani, J., and Flandro, G. A., "Fundamental Growth Rate Corrections in Rocket Motor Stability Calculations," AIAA Paper 2002-3610, July 2002.

[5]Fischbach, S. R., Flandro, G. A., and Majdalani, J., "Volume-to-Surface Transformations of Rocket Stability Integrals," AIAA Paper 2004-4053, July 2004.

[6]Blomshield, F. S., Mathes, H. B., Crump, J. E., Beiter, C. A., and Beckstead, M. W., "Nonlinear Stability Testing of Full-Scale Tactical Motors," *Journal of Propulsion and Power,* Vol. 13, No. 3, 1997, pp. 356-366.

[7]Blomshield, F. S., "Stability Testing and Pulsing of Full Scale Tactical Motors, Parts I and II," Naval Air Warfare Center, NAWCWPNS TP 8060, February 1996.

[8]Blomshield, F. S., Bicker, C. J., and Stalnaker, R. A., "High Pressure Pulsed Motor Firing Combustion Instability Investigations," *Proceedings of the 1996 JANNAF 33rd Combustion Meeting*, Naval Postgraduate School, Monterey, CA, 1996.

[9]Blomshield, F. S., Crump, J. E., Mathes, H. B., Stalnaker, R. A., and Beckstead, M. W., "Stability Testing of Full-Scale Tactical Motors," *Journal of Propulsion and Power,* Vol. 13, No. 3, 1997, pp. 349-355.

[10]Blomshield, F. S., and Mathes, H. B., "Pressure Oscillations in Post-Challenger Space Shuttle Redesigned Solid Rocket Motors," *Journal of Propulsion and Power,* Vol. 9, No. 2, 1993, pp. 217-221.

[11]Apte, S., and Yang, V., "Unsteady Flow Evolution in a Porous Chamber with Surface Mass Injection. Part I: Free Oscillation," *AIAA Journal,* Vol. 39, No. 8, 2001, pp. 1577-1586.

[12]Apte, S., and Yang, V., "Unsteady Flow Evolution in a Porous Chamber with Surface Mass Injection. Part II: Acoustic Excitation," *AIAA Journal,* Vol. 40, No. 2, 2002, pp. 244-253.

[13]Casalis, G., Avalon, G., and Pineau, J.-P., "Spatial Instability of Planar Channel Flow with Fluid Injection through Porous Walls," *The Physics of Fluids,* Vol. 10, No. 10, 1998, pp. 2558-2568.

[14]Griffond, J., and Casalis, G., "On the Dependence on the Formulation of Some Nonparallel Stability Approaches Applied to the Taylor Flow," *The Physics of Fluids,* Vol. 12, No. 2, 2000, pp. 466-468.

[15]Griffond, J., and Casalis, G., "On the Nonparallel Stability of the Injection Induced Two-Dimensional Taylor Flow," *The Physics of Fluids,* Vol. 13, No. 6, 2001, pp. 1635-1644.

[16]Avalon, G., Casalis, G., and Griffond, J., "Flow Instabilities and Acoustic Resonance of Channels with Wall Injection," AIAA Paper 98-3218, July 1998.

[17]Liou, T. M., Lien, W. Y., and Hwang, P. W., "Large-Eddy Simulations of Turbulent Reacting Flows in a Chamber with Gaseous Ethylene Injecting through the Porous Wall," *Combustion and Flame,* Vol. 99, No. 3-4, 1994, pp. 591-600.

[18]Liou, T. M., Lien, W. Y., and Hwang, P. W., "Transition Characteristics of Flowfield in a Simulated Solid-Rocket Motor," *Journal of Propulsion and Power,* Vol. 14, No. 3, 1998, pp. 282-289.

[19]Liou, T.-M., and Lien, W.-Y., "Numerical Simulations of Injection-Driven Flows in a Two-Dimensional Nozzleless Solid-Rocket Motor," *Journal of Propulsion and Power,* Vol. 11, No. 4, 1995, pp. 600-606.

[20]Vuillot, F., and Lupoglazoff, N., "Combustion and Turbulent Flow Effects in 2-D Unsteady Navier-Stokes Simulations of Oscillatory Rocket Motors," AIAA Paper 96-0884, January 1996.

[21]Vuillot, F., Dupays, J., Lupoglazoff, N., Basset, T., and Daniel, E., "2-D Navier-Stokes Stability Computations for Solid Rocket Motors: Rotational, Combustion and Two-Phase Flow Effects," AIAA Paper 97-3326, July 1997.

[22]Prévost, M., Vuillot, F., and Traineau, J. C., "Vortex-Shedding Driven Oscillations in Subscale Motors for the Ariane 5 MPS Solid Rocket Motors," AIAA Paper 96-3247, July 1996.

[23]Lupoglazoff, N., and Vuillot, F., "Numerical Simulation of Vortex Shedding Phenomenon in Two-Dimensional Test Case Solid Rocket Motors," AIAA Paper 92-0776, January 1992.

[24]Couton, D., Doan-Kim, S., and Vuillot, F., "Numerical Simulation of Vortex-Shedding Phenomenon in a Channel with Flow Induced through Porous Wall," *International Journal of Heat and Fluid Flow,* Vol. 18, No. 3, 1997, pp. 283-296.

[25]Ugurtas, B., Avalon, G., Lupoglazoff, N., and Vuillot, F., "Numerical Computations of Hydrodynamic Instabilities inside Channels with Wall Injection," AIAA Paper 99-2505, June 1999.

[26]Flandro, G. A., "On Flow Turning," AIAA Paper 95-2530, July 1995.

[27]Flandro, G. A., "Effects of Vorticity on Rocket Combustion Stability," *Journal of Propulsion and Power,* Vol. 11, No. 4, 1995, pp. 607-625.

[28]Majdalani, J., "Modeling of the Oscillatory Flowfield between Two Parallel Plates with Sidewall Injection," AIAA Paper 98-2977, June 1998.

[29]Majdalani, J., "A Novel Flowfield Solution in a Rectangular Cavity Subject to Small Amplitude Oscillations," 2nd AIAA Theoretical Fluid Mechanics Meeting Paper AIAA 98-2693, June 1998.

[30]Majdalani, J., "Asymptotic Formulation for an Acoustically Driven Field inside a Rectangular Cavity with a Well-Defined Convective Mean Flow Motion," *Journal of Sound and Vibration,* Vol. 223, No. 1, 1999, pp. 73-95.

[31]Flandro, G. A., and Majdalani, J., "Aeroacoustic Instability in Rockets," AIAA Paper 2001-3868, July 2001.

[32]White, F. M., *Viscous Fluid Flow*, McGraw-Hill, New York, 1991, pp. 135-136.

[33]Majdalani, J., "The Boundary Layer Structure in Cylindrical Rocket Motors," *AIAA Journal,* Vol. 37, No. 4, 1999, pp. 505-508.

[34]Majdalani, J., and Roh, T. S., "The Oscillatory Channel Flow with Large Wall Injection," *Proceedings of the Royal Society, Series A,* Vol. 456, No. 1999, 2000, pp. 1625-1657.

[35]Price, E. W., "Velocity Coupling in Oscillatory Combustion of Solid Propellants," *AIAA Journal,* Vol. 17, No. 7, 1983, pp. 799-800.

[36]Flandro, G. A., "Effects of Vorticity Transport on Axial Acoustic Waves in a Solid Propellant Rocket Chamber," *Combustion Instabilities Driven by Thermo-Chemical Acoustic Sources*, Vol. NCA 4, HTD 128, American Society of Mechanical Engineers, New York, 1989, pp. 53-61.

[37]Flanagan, S. N., Flandro, G. A., and Thomas, H. D., "A New Approach to Velocity Coupling," AIAA Paper 97-2734, July 1995.

[38]Flandro, G. A., "Nonlinear Combustion of a Solid Propellant with Velocity Coupling," AIAA Paper 83-1269, June 1983.

[39]Culick, F. E. C., "Stability of Longitudinal Oscillations with Pressure and Velocity Coupling in a Solid Propellant Rocket," *Combustion Science and Technology,* Vol. 2, No. 4, 1970, pp. 179-201.

[40]Ananthkrishnan, N., "Qualitative Dynamics of Nonlinear Acoustic Waves in a Combustion Chamber, III: Velocity Coupling Models," Guggenheim Jet Propulsion Center, California Institute of Technology, Guggenheim Jet Propulsion Center documents on active control of combustion instabilities Rept. CI 01-01, Pasadena, CA2001.

[41]Isella, G., and Culick, F. E. C., "Modelling the Effects of Velocity Coupling on the Global Dynamics of Combustion Chambers," AIAA Paper 2000-3187, 2000.

[42]Ma, Y., Van Moorhem, W. K., and Shorthill, R. W., "Innovative Method of Investigating the Role of Turbulence in the Velocity Coupling Phenomenon," *Journal of Vibration and Acoustics-Transactions of the ASME,* Vol. 112, No. 4, 1990, pp. 550-555.

[43]Ma, Y., Van Moorhem, W. K., and Shorthill, R. W., "Experimental Investigation of Velocity Coupling in Combustion Instability," *Journal of Propulsion and Power,* Vol. 7, No. 5, 1991, pp. 692-699.

[44]Flandro, G. A., Fischbach, S. R., Majdalani, J., and French, J. C., "Nonlinear Rocket Motor Stability Prediction: Limit Amplitude, Triggering, and Mean Pressure Shift," AIAA Paper 2004-4054, July 2004.